

Analysis of the Nicolson-Ross-Weir Method for Characterizing the Electromagnetic Properties of Engineered Materials

Edward J. Rothwell^{1,*}, Jonathan L. Frasch¹, Sean M. Ellison¹,
Premjeet Chahal¹, and Raoul O. Ouedraogo²

Abstract—A method for predicting the behavior of the permittivity and permeability of an engineered material by examining the measured S -parameters of a material sample is devised, assuming that the sample is lossless and symmetric. The S -parameter conditions under which the material parameters extracted using the Nicolson-Ross-Weir method may be associated with a lossless homogeneous material are described. Also, the relationship between the signs of the real and imaginary parts of the permittivity and permeability are determined, both when the extracted material parameters are real and when they are complex. In particular, the conditions under which metamaterials exhibit double-negative properties may be predicted from the S -parameters of a metamaterial sample. The relationships between material characteristics and the S -parameters should prove useful when synthesizing materials to have certain desired properties. Examples, both from experiment and simulation, demonstrate that the relationships may be used to understand the behavior of several different categories of engineered materials, even when the materials have appreciable loss.

1. INTRODUCTION

The Nicolson-Ross-Weir (NRW) method has, for more than forty years, been a standard technique for measuring the permittivity and permeability of homogeneous, isotropic materials [1–4]. The method is robust to most common sources of experimental error, and utilizes closed form expressions for the desired material properties that are computed from measured S -parameters. Recently, the NRW method has also been applied to manufactured materials, notably polymer composites with magnetic inclusions [5–7], but also more exotic engineered materials such as carbon nanotube films [8, 9], and composite layered dielectrics [10]. Particularly interesting is the use of the NRW method as a homogenization method for metamaterials and for studying metamaterial elements [11]. Although this approach has some difficulties [12, 13], it has been used to great effect to characterize the metamaterial elements used in many novel antennas [13–17].

Because the NRW method relies on closed-form expressions, it is possible to perform an analysis to predict the behavior of the extracted material parameters by directly examining the measured S -parameters. For general materials, these expressions are too complicated to deduce any simple relationships. However, if the engineered material is assumed to be lossless, isotropic, and symmetric, some very important properties of the extracted material parameters can be easily deduced. In particular, it is possible to tell the circumstances under which the extracted material parameters may be interpreted as arising from a lossless homogeneous material. It is also possible to determine the relationship between the signs of the real and imaginary parts of ϵ and μ when the extracted material parameters are either real or complex. These characteristics are very useful when synthesizing materials

Received 17 July 2016, Accepted 2 October 2016, Scheduled 10 October 2016

* Corresponding author: Edward J. Rothwell (rothwell@egr.msu.edu).

¹ Department of Electrical and Computer Engineering, Michigan State University, East Lansing, MI 48824-1226, USA. ² MIT Lincoln Laboratory, 244 Wood Street, Lexington, MA 02420, USA.

to have certain properties, since it is possible to place constraints on the S -parameters in order to achieve a certain desired material behavior.

Although most engineered materials are not lossless, some interesting structures are made purely from metallic elements, and may be approximated as lossless. For instance, the magnetic waveguide material standard described in [18] is metallic. Some of the basic observations described here were first identified in the analysis of that structure. Also, some newer metamaterials, particularly those designed for high power purposes, are constructed entirely of metal [19, 20]. Although the analysis in this paper is only valid for lossless structures, it can still be used to understand and predict the behavior of engineered materials with low to moderate loss. To demonstrate this, a metamaterial insert is considered in Section 6 that has appreciable loss near resonance. Other examples include a layered material and a waveguide aperture. These results all demonstrate that the analysis presented here is useful for understanding the properties of engineered materials based on the behavior of their S -parameters.

In brief, the purpose of this paper is to establish a relationship between the S -parameters of a measured system, and the properties of the permittivity and permeability extracted from the S -parameters using NRW. The conditions on the S -parameters for which the imaginary parts of the extracted material parameters are zero are established. The conditions on the S -parameters that determine the signs of both the real and imaginary parts of the extracted material parameters are also determined. In the present study, the S -parameters are assumed to those of a lossless, symmetric, reciprocal 2-port network.

The structure of the paper is as follows. Section 2 provides an overview of NRW, and gives the closed form extraction equations for the most common implementations: free-space systems, TEM waveguiding systems, and rectangular waveguide systems. Section 3 provides a derivation of the desired conditions on the S -parameters. Section 4 examines a numerical example of a layered material in a TEM waveguiding system, and demonstrates how the S -parameters can be used to predict the behavior of the extracted material parameters. Section 5 uses S -parameter measurements of an iris in a rectangular waveguide to validate with experimental data the relationships determined in Section 3. Section 6 shows that the relationships can be helpful when characterizing metamaterial structures, even when those structures have nonzero loss, by considering simulations of a metamaterial insert in a rectangular waveguide. Finally, Section 7 provides a summary and a discussion of applying the relationships in practical situations.

2. THE NICOLSON-ROSS-WEIR METHOD

The NRW method is based on measuring the reflection from, and transmission through, a homogeneous sample of isotropic material under specified illumination conditions. The material has complex permittivity $\epsilon(\omega) = \epsilon_r(\omega)\epsilon_0 = \epsilon'(\omega) - j\epsilon''(\omega)$ and permeability $\mu(\omega) = \mu_r(\omega)\mu_0 = \mu'(\omega) - j\mu''(\omega)$ and occupies the region between the planes $z = 0$ and $z = d$, while the regions $z < 0$ and $z > d$ are assumed to be free space. The sample is illuminated by a wave originating from $z < 0$. Three specific implementations are contemplated. In the first, the material is illuminated in free space by either a parallel or perpendicular-polarized plane wave that is incident at an angle θ_0 from the normal to the material. In this case the material is assumed to be infinite in the x and y -directions. In the second implementation, the material occupies a guided wave structure that is operated in the TEM mode, such as a coaxial cable or a stripline. In this case it is assumed that the material completely fills the cross section of the structure, and that only the TEM mode is present in all regions. In the third implementation, the material occupies a guiding wave structure with either a single TE or TM mode present in all regions. In this study, the specific case of a TE_{10} mode in a rectangular waveguide of width a and height b is considered. The goal of the NRW method is to determine ϵ and μ using measurements of the reflection coefficient (S_{11}) and the transmission coefficient (S_{21}), as defined as the ratio of reflected or transmitted transverse electric field to incident transverse electric field at the planes of the material sample.

In all three cases the S -parameters may be written as

$$S_{11} = \frac{(1 - P^2)\Gamma}{1 - P^2\Gamma^2}, \quad S_{21} = \frac{(1 - \Gamma^2)P}{1 - P^2\Gamma^2}. \quad (1)$$

Here P is the propagation factor given by

$$P = e^{-jk_z d} \quad (2)$$

where k_z is the z -component of the propagation vector defined through

$$k_z^2 = k^2 - \kappa^2. \quad (3)$$

Here $k = \omega\sqrt{\mu\epsilon}$ is the wavenumber in the material, and $\kappa = 0$ for TEM guided-wave systems, $\kappa = k_0 \sin \theta_0$ for free-space systems where $k_0 = \omega\sqrt{\mu_0\epsilon_0}$, and $\kappa = \pi/a$ for TE_{10} -mode rectangular waveguide systems. Additionally, Γ is the interfacial reflection coefficient given by

$$\Gamma = \frac{Z - Z_0}{Z + Z_0}. \quad (4)$$

For TEM guided-wave systems, $Z = \eta$ and $Z_0 = \eta_0$, where $\eta = \sqrt{\mu/\epsilon}$ and $\eta_0 = \sqrt{\mu_0/\epsilon_0}$. For TE_{10} -mode rectangular waveguide systems, $Z = \omega\mu/k_z$ and $Z_0 = \omega\mu_0/k_{z0}$, where $k_{z0}^2 = k_0^2 - \kappa^2$. For the free-space method the transverse wave impedances are

$$Z = \begin{cases} \frac{k\eta}{k_z}, & \perp\text{-pol}, \\ \frac{k_z\eta}{k}, & \parallel\text{-pol}, \end{cases} \quad Z_0 = \begin{cases} \frac{\eta_0}{\cos \theta_0}, & \perp\text{-pol}, \\ \eta_0 \cos \theta_0, & \parallel\text{-pol}. \end{cases} \quad (5)$$

The NRW method was proposed in the original work of Nicolson and Ross [1] and of Weir [2]. Begin by defining intermediate quantities

$$V_1 = S_{21} + S_{11} = \frac{P + \Gamma}{1 + \Gamma P}, \quad V_2 = S_{21} - S_{11} = \frac{P - \Gamma}{1 - \Gamma P}. \quad (6)$$

The quantities P and Γ may be determined in terms of the measured quantities S_{11} and S_{21} by rearranging these expressions. First P is eliminated from the equations, resulting in a quadratic equation for Γ ,

$$\Gamma^2 - 2\Gamma X + 1 = 0, \quad (7)$$

where

$$X = \frac{1 - V_1 V_2}{V_1 - V_2} = \frac{1 - S_{21}^2 + S_{11}^2}{2S_{11}}. \quad (8)$$

The solution is

$$\Gamma = X + s_1 \sqrt{X^2 - 1}, \quad (9)$$

where $s_1 = \pm 1$. The sign ambiguity is usually resolved by assuming that the material is passive, since only one choice of sign satisfies the inequality $|\Gamma| \leq 1$. Once Γ is determined, P is easily found as

$$P = \frac{V_1 - \Gamma}{1 - V_1 \Gamma} = |P| e^{j\phi}, \quad (10)$$

where $-\pi < \phi \leq \pi$. Equating Eq. (10) to Eq. (2) and defining the dimensionless quantity $\bar{k}_z = k_z/k_0$, k_z is found by taking the natural logarithm:

$$\bar{k}_z = \frac{n - \frac{\phi}{2\pi}}{d/\lambda_0} + j \frac{\ln |P|/2\pi}{d/\lambda_0}. \quad (11)$$

Here $\lambda_0 = f/c$ is the free-space wavelength. This equation reveals one of the known difficulties with the NRW method. The integer n defines the branch of the log function. Its value is not known a priori, but is related to the electrical thickness of the sample. Since the material parameters are unknown, n may be difficult to determine unless some test against known physics is employed, such as $\epsilon'' > 0$ for passive materials. For engineered materials, however, this test may not be applicable. The reference [21] presents a detailed discussion of this problem with suggestions for its resolution.

With \bar{k}_z known, μ and ϵ are determined as follows. First define

$$F = \frac{1 - \Gamma}{1 + \Gamma}. \quad (12)$$

Then, for TEM waveguiding systems,

$$\epsilon_r = \bar{k}_z F, \quad \mu_r = \frac{\bar{k}_z}{F}. \quad (13)$$

Otherwise, compute

$$\bar{k}^2 = \bar{k}_z^2 + \bar{\kappa}^2, \quad (14)$$

where $\bar{\kappa} = \kappa/k_0$. Then, for a TE₁₀ rectangular waveguide system

$$\epsilon_r = \bar{k}^2 \frac{\bar{k}_{z0} F}{\bar{k}_z}, \quad \mu_r = \frac{\bar{k}_z}{\bar{k}_{z0} F}, \quad (15)$$

where $\bar{k}_{z0} = k_{z0}/k_0$. For a free-space system with perpendicular polarization,

$$\epsilon_r = \frac{\bar{k}^2 F \cos \theta_0}{\bar{k}_z}, \quad \mu_r = \frac{\bar{k}_z}{F \cos \theta_0}. \quad (16)$$

Finally, for a free-space system with parallel polarization,

$$\epsilon_r = \frac{\bar{k}_z F}{\cos \theta_0}, \quad \mu_r = \frac{\bar{k}^2 \cos \theta_0}{\bar{k}_z F}. \quad (17)$$

Note that for a free space system with normal incidence ($\theta_0 = 0$), the equations for μ_r and ϵ_r reduce to those of a TEM system.

3. NRW FOR A LOSSLESS, RECIPROCAL, SYMMETRIC ENGINEERED MATERIAL

Many engineered materials are made by etching metallic parts on circuit boards, or by embedding metallic elements into a low loss dielectric matrix [22]. Some specific structures may be made from metallic elements in vacuum or air [18]. Although there will always be some small metallic or dielectric losses associated with all non-superconducting metamaterials, the assumption of a lossless material greatly simplifies the analysis of the NRW method. By also assuming that the engineered material is reciprocal and symmetric, resulting conditions on the S -parameters can be used to determine the relationship between the extracted values of μ and ϵ and the S -parameters themselves. This should prove useful for those wishing to synthesize a material with certain properties.

The assumed conditions for the engineered material are:

- (i) Reciprocity: $S_{21} = S_{12}$;
- (ii) Symmetry: $S_{11} = S_{22}$;
- (iii) Lossless.

3.1. Conditions on S -Parameters

With the assumptions above, the S -parameters for the engineered material must obey certain properties. For any single-mode 2-port network, the power dissipated is given by [23]

$$P_{\text{diss}} = \frac{1}{2} a^T Q a^*, \quad (18)$$

where a is the 2-vector of wave amplitudes entering the network, and Q is the 2×2 *dissipation matrix* $Q = I - S^T S^*$ with I the identity matrix. If the 2-port network is lossless then $P_{\text{diss}} = 0$ and thus $Q = 0$ and the S -parameters obey the unitary property

$$S^T S^* = I. \quad (19)$$

Writing out the matrix product gives the three conditions

$$|S_{11}|^2 + |S_{21}|^2 = 1, \quad (20)$$

$$|S_{12}|^2 + |S_{22}|^2 = 1, \quad (21)$$

$$S_{11} S_{12}^* + S_{21} S_{22}^* = 0. \quad (22)$$

From Eq. (22) it is evident that

$$|S_{22}|^2 = |S_{11}|^2 \frac{|S_{12}|^2}{|S_{21}|^2}. \quad (23)$$

Substituting Eqs. (20) and (21) then gives

$$|S_{22}| = |S_{11}|, \quad |S_{21}|^2 = 1 - |S_{11}|^2, \quad |S_{12}|^2 = 1 - |S_{22}|^2. \quad (24)$$

If ϕ_{ij} is the phase of S_{ij} , then Eq. (22) provides the relationship

$$\phi_{11} - \phi_{12} - \phi_{21} + \phi_{22} \pm \pi = 0, \quad (25)$$

and thus only 1 amplitude, 3 phases, and a choice of sign are required to specify all 4 complex S -parameters. If, in addition, the system is reciprocal, such that $\phi_{12} = \phi_{21}$, then only 2 phases are required. Finally, if the system is also symmetric, such that $\phi_{11} = \phi_{22}$, only a single amplitude and phase (and a sign selection) are required to specify all 4 complex S -parameters. In this case the phase relationship is

$$\phi_{11} - \phi_{21} \pm \frac{\pi}{2} = 0. \quad (26)$$

Combining Eqs. (20) and (26) provides the relationship that will be used to study the NRW method:

$$S_{21} = js_0 S_{11} M, \quad (27)$$

where $s_0 = \pm 1$ and

$$M = \sqrt{\frac{1 - |S_{11}|^2}{|S_{11}|^2}}. \quad (28)$$

The presence of s_0 shows that for each value of S_{11} , there are two possible values of S_{21} that satisfy the conditions of a lossless, reciprocal, and symmetric network.

From Eq. (6) it is evident that

$$V_1 = S_{21} + S_{11} = S_{11} [1 + js_0 M], \quad (29)$$

and so

$$V_{1r} = S_{11r} - s_0 S_{11i} M, \quad V_{1i} = S_{11i} + s_0 S_{11r} M, \quad (30)$$

where $V_1 = V_{1r} + jV_{1i}$. Thus,

$$|V_1|^2 = |S_{11}|^2 [1 + M^2] = 1. \quad (31)$$

Note that the effect of the sign s_0 is to reflect the real part of V_1 through the real S_{11} axis, and to reflect the imaginary part of V_1 through the imaginary S_{11} axis. That is, a change in s_0 accompanied by a change of sign in S_{11i} will maintain the value of V_{1r} , while a change in s_0 accompanied by a change of sign in S_{11r} will maintain the value of V_{1i} .

3.2. Relationship of μ and ϵ to S_{11}

Substituting Eq. (27) into Eq. (8), it is found that X is a real quantity given by

$$X = \Re \left\{ \frac{1}{S_{11}} \right\} = \frac{S_{11r}}{|S_{11}|^2} = \frac{\cos \phi_{11}}{|S_{11}|}. \quad (32)$$

Thus, X may take on all real values: $-\infty < X < \infty$. Note that the choice of the sign s_0 does not affect the value of X , and that X has odd symmetry about the imaginary S_{11} axis.

The analysis is separated into two cases for X which yield two classes of physical behavior for ϵ and μ : $X^2 \geq 1$ and $X^2 < 1$. The boundary between these two cases is determined by the curve $|S_{11}| = |\cos \phi|$, which is shown in Figure 2 as the two adjacent circles in the complex S -plane. The points within and on these circles correspond to the case $X^2 \geq 1$, while the points external correspond to $X^2 < 1$.

Table 1. Values of Γ resulting from two conditions on X and the choice of sign in Equation (9).

	$X \geq 1$	$X \leq -1$
$s_1 = 1$	$1 \leq \Gamma$	$-1 \leq \Gamma < 0$
$s_1 = -1$	$0 < \Gamma \leq 1$	$\Gamma \leq -1$

Case 1: $X^2 \geq 1$

From Eq. (9) it is seen that when $X^2 \geq 1$, Γ is real. The ranges of values taken on by Γ for the subcases $X \geq 1$ and $X \leq -1$ are shown in Table 1. Whether or not $|\Gamma| \leq 1$, which is the condition enforced in the standard NRW approach, depends on the sign s_1 chosen in Eq. (9).

When $X = 1$, $\Gamma = 1$ from Eq. (9). Also, from Eq. (8),

$$V_1 - V_2 + V_1 V_2 - 1 = (V_1 - 1)(V_2 + 1) = 0, \quad (33)$$

which is satisfied by $S_{21} = 0$ and $S_{11} = 1$. Similarly, when $X = -1$, $\Gamma = -1$, and

$$V_2 - V_1 + V_1 V_2 - 1 = (V_2 - 1)(V_1 + 1) = 0, \quad (34)$$

which is satisfied by $S_{21} = 0$ and $S_{11} = -1$. Thus, the cases $X = 1$ and $X = -1$ represent total reflection from the material interface.

For values of X satisfying $X^2 > 1$, note that since X is real,

$$F = \frac{1 - X - s_1 \sqrt{X^2 - 1}}{1 + X + s_1 \sqrt{X^2 - 1}} = \begin{cases} -s_1 \sqrt{\frac{X-1}{X+1}}, & X > 1, \\ s_1 \sqrt{\frac{X-1}{X+1}}, & X < -1. \end{cases} \quad (35)$$

Thus the quantity F , which appears in all of the expressions for μ and ϵ , is real and has a sign determined by s_1 . Clearly F becomes unbounded as $X \rightarrow -1$.

Using Table 1 gives the values

$$F = \begin{cases} +\sqrt{\frac{X-1}{X+1}}, & |\Gamma| < 1, \\ -\sqrt{\frac{X-1}{X+1}}, & |\Gamma| > 1. \end{cases} \quad (36)$$

Thus, enforcing the usual NRW condition that $|\Gamma| < 1$ produces a positive value of F .

The quantity P may be computed from Eq. (10):

$$P = \frac{(V_{1r} - \Gamma) + jV_{1i}}{(1 - \Gamma V_{1r}) - j\Gamma V_{1i}} = \frac{(X V_{1r} - 1) + jV_{1i} (1/\Gamma - X)}{X - V_{1r}}. \quad (37)$$

The magnitude of P is found from

$$\begin{aligned} |P|^2 &= \left| \frac{(V_{1r} - \Gamma) + jV_{1i}}{(1 - \Gamma V_{1r}) - j\Gamma V_{1i}} \right|^2 \\ &= \left[\frac{V_{1r}^2 + V_{1i}^2 - 2\Gamma V_{1r} + \Gamma^2}{1 + \Gamma^2 V_{1r}^2 - 2\Gamma V_{1r} + \Gamma^2 V_{1i}^2} \right] = 1 \end{aligned} \quad (38)$$

since $|V_1|^2 = 1$. Because $|P| = 1$, it is evident from Eq. (11) that \bar{k}_z is purely real:

$$\bar{k}_z = \frac{n - \frac{\phi}{2\pi}}{d/\lambda_0}. \quad (39)$$

The phase of P is found from Eq. (37) as

$$\tan \phi = V_{1i} \frac{1/\Gamma - X}{X V_{1r} - 1} = -s_1 V_{1i} \frac{\sqrt{X^2 - 1}}{X V_{1r} - 1}. \quad (40)$$

Note that the product XV_{1r} is given by

$$XV_{1r} = \frac{S_{11r}^2}{|S_{11}|^2} - s_0 \frac{S_{11r}S_{11i}}{|S_{11}|^2} M. \quad (41)$$

Thus, a change in s_0 accompanied by *either* a change in sign of S_{11r} or S_{11i} maintains the value of XV_{1r} . Similarly, it was shown earlier that a change in s_0 accompanied by a change in sign of S_{11r} will maintain the value of V_{1i} . Thus, the four possible combinations of s_0 and s_1 , as outlined in Table 3, will produce four distinct symmetry states for ϕ . In each case the values of ϕ range from $-\pi$ to π with no duplicated values. Thus, each case gives identical values of μ and ϵ , except that the values are associated with different, but symmetric, positions in the complex S_{11} plane.

At this point the following conclusions can be made about ϵ and μ from Eqs. (13)–(17):

- (i) Both ϵ and μ are real;
- (ii) The sign of ϵ is the same as the sign of μ , which is the sign of $\bar{k}_z F$.

As an example, select $n = 0$. Then the sign of \bar{k}_z is the opposite of the sign of ϕ . Since the sign on F is given by Eq. (35), the signs of ϵ and μ are given in Table 2. The case of ($|\Gamma| < 1, -\pi < \phi < 0$) produces positive values of ϵ and μ , and represents a phase change of less than 180° for propagation through the sample. This is what is expected of an ordinary material less than a half wavelength in thickness, as is the standard situation for using NRW. More interesting, the case of ($|\Gamma| < 1, 0 < \phi < \pi$) produces negative ϵ and μ . If Δ is less than a half wavelength, this combination may be interpreted as having the properties of a lossless double-negative metamaterial. While the magnitude of the reflection coefficient is less than unity, the phase change through the material is positive.

Table 2. Sign of both ϵ and μ for $n = 0$.

	$ \Gamma < 1$	$ \Gamma > 1$
$-\pi < \phi < 0$	+	-
$0 < \phi < \pi$	-	+

Table 3. Signs for the four possible cases for ϕ with $X^2 > 1$ and for P with $X^2 < 1$.

Case	s_0	s_1 or s_2
A	+	+
B	+	-
C	-	+
D	-	-

Case 2: $X^2 < 1$

From (9) it is seen that when $X^2 < 1$, Γ is a complex number given by

$$\Gamma = X + js_2\sqrt{1 - X^2}, \quad (42)$$

where $s_2 = \pm 1$. It is immediately obvious that

$$|\Gamma|^2 = X^2 + 1 - X^2 = 1, \quad (43)$$

and thus this case represents total interfacial reflection.

The quantity P is again computed from Eq. (10), giving

$$P = \frac{V_{1r} - X}{1 - V_{1r}X + s_2V_{1i}\sqrt{1 - X^2}}. \quad (44)$$

Thus P is real, with the phase ϕ determined purely by the sign of P . As with ϕ when $X^2 \geq 1$, the signs s_0 and s_2 produce four symmetry cases, which are shown in Table 3.

The value of F may be determined from

$$F = \frac{1 - \Gamma}{1 + \Gamma} = \frac{(1 - X) - js_2\sqrt{1 - X^2}}{(1 + X) + js_2\sqrt{1 - X^2}} = -js_2\sqrt{\frac{1 - X}{1 + X}}. \quad (45)$$

Thus $F = jF_i$ is always imaginary when $X^2 < 1$; clearly F_i is unbounded as $X \rightarrow -1$.

With these values, the behavior of μ and ϵ can now be examined. For the case of a TEM system, Eq. (13) gives

$$\epsilon_r = -\bar{k}_{zi}F_i + j\bar{k}_{zr}F_i, \quad (46)$$

$$\mu_r = \frac{\bar{k}_{zi}}{F_i} - j\frac{\bar{k}_{zr}}{F_i}. \quad (47)$$

Thus, the real parts of the extracted ϵ and μ will always have opposite signs, as will the imaginary parts. In fact, it is seen that

$$\frac{\mu_r}{\epsilon_r} = -\frac{1}{F_i^2} < 0, \quad (48)$$

and thus $\eta = \sqrt{\mu/\epsilon} = j\eta_i$ is purely imaginary. Then

$$\Gamma = \frac{\eta - \eta_0}{\eta + \eta_0} = \frac{j\eta_i - \eta_0}{j\eta_i + \eta_0}, \quad (49)$$

and $|\Gamma| = 1$, indicating total interfacial reflection. Substituting Eqs. (11) and (45) gives specific formulas for ϵ_r and μ_r :

$$\epsilon_r = s_2 \frac{\ln |P|/2\pi}{d/\lambda_0} \sqrt{\frac{1 - X}{1 + X}} - js_2 \frac{n - \frac{\phi}{2\pi}}{d/\lambda_0} \sqrt{\frac{1 - X}{1 + X}}, \quad (50)$$

$$\mu_r = -s_2 \frac{\ln |P|/2\pi}{d/\lambda_0} \sqrt{\frac{1 + X}{1 - X}} + js_2 \frac{n - \frac{\phi}{2\pi}}{d/\lambda_0} \sqrt{\frac{1 + X}{1 - X}}. \quad (51)$$

Thus, if $n = 0$ is chosen, and $P > 0$, the permittivity and permeability will both be real. However, one will be positive, and one will be negative.

For the case of a TE₁₀ mode rectangular waveguide system, Eq. (15) gives

$$\epsilon_r = -\bar{k}_{zi}\bar{k}_{z0}F_i \left(1 - \frac{\bar{\kappa}^2}{|\bar{k}_z|^2} \right) + j\bar{k}_{zr}\bar{k}_{z0}F_i \left(1 + \frac{\bar{\kappa}^2}{|\bar{k}_z|^2} \right), \quad (52)$$

$$\mu_r = \frac{\bar{k}_{zi}}{\bar{k}_{z0}F_i} - j\frac{\bar{k}_{zr}}{\bar{k}_{z0}F_i}. \quad (53)$$

Thus, the real parts of μ and ϵ will have the same sign if $|\bar{k}_z|^2 < \bar{\kappa}^2$. However, the imaginary parts will always have opposite signs. For the case of a free-space system with perpendicular polarization, Eq. (16) gives

$$\epsilon_r = -\bar{k}_{zi}F_i \cos \theta_0 \left(1 - \frac{\sin^2 \theta_0}{|\bar{k}_z|^2} \right) + j\bar{k}_{zr}F_i \cos \theta_0 \left(1 + \frac{\sin^2 \theta_0}{|\bar{k}_z|^2} \right), \quad (54)$$

$$\mu_r = \frac{\bar{k}_{zi}}{F_i \cos \theta_0} - j\frac{\bar{k}_{zr}}{F_i \cos \theta_0}, \quad (55)$$

while for the case of parallel polarization, Eq. (17) gives

$$\epsilon_r = -\frac{\bar{k}_{zi}F_i}{\cos \theta_0} + j\frac{\bar{k}_{zr}F_i}{\cos \theta_0}, \quad (56)$$

$$\mu_r = \frac{\bar{k}_{zi} \cos \theta_0}{F_i} \left(1 - \frac{\sin^2 \theta_0}{|\bar{k}_z|^2} \right) - j\frac{\bar{k}_{zr} \cos \theta_0}{F_i} \left(1 + \frac{\sin^2 \theta_0}{|\bar{k}_z|^2} \right). \quad (57)$$

Similar to the TE₁₀ waveguide mode case, the real parts of μ and ϵ will have the same sign if $|\bar{k}_z|^2 < \sin^2 \theta_0$. However, the imaginary parts will always have opposite signs.

4. EXAMPLE 1: LAYERED DIELECTRIC MATERIAL

As a first, purely numerical example, consider a layered dielectric sample placed into a TEM system (either a waveguiding system, or a free space system under normal incidence). The sample consists of a layer of material with thickness Δ and relative permittivity $\epsilon_r = 10$ embedded and centered within a layer of relative permittivity $\epsilon_r = 2$, as shown in Figure 1. The total thickness of the sample is $d = 2$ cm, and the thickness ratio is defined as $\tau = \Delta/d$, $0 \leq \tau \leq 1$. Figure 2 shows a plot of S_{11} at $f = 2$ GHz and $f = 3$ GHz, computed at the sample planes using a cascaded layer method. Since the layers are lossless, the value of S_{21} is related to S_{11} through Eq. (27). At 2 GHz it is found that $s_0 = 1$ for all values of τ . At 3 GHz, $s_0 = 1$ for $0 < \tau \leq 0.763$, and $s_0 = -1$ for $\tau \geq 0.764$.

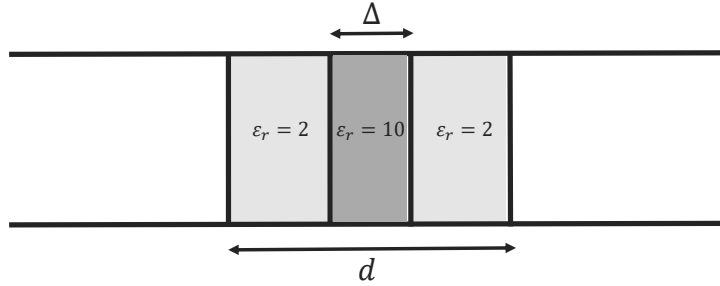


Figure 1. Layered dielectric in a TEM system.

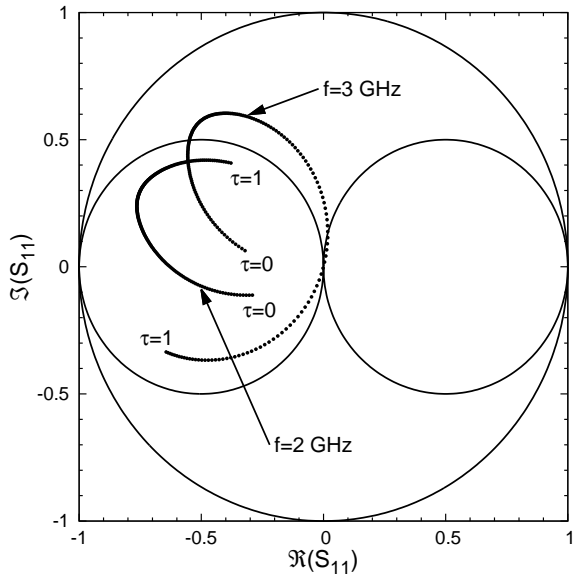


Figure 2. S_{11} for a layered dielectric material in a TEM system.

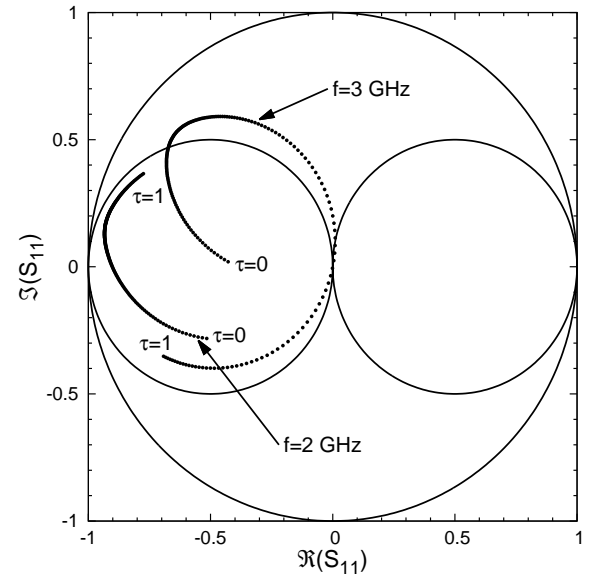


Figure 3. S_{11} for a layered dielectric material in a WR340 rectangular waveguide.

Figure 2 provides some immediate feedback about the behavior of the values of μ and ϵ extracted using the NRW method. When $f = 2$ GHz, all values of S_{11} reside in the region where $X < -1$, and thus extracted values of μ and ϵ are real for all values of τ . Figure 4 shows μ and ϵ as a function of τ , extracted using (13) at $f = 2$ GHz with $n = 0$. When $\tau = 0$ the sample is homogeneous, with a relative permittivity of $\epsilon_r = 2$. When $\tau = 1$ the sample is homogeneous, with a relative permittivity of $\epsilon_r = 10$. In between these values the extracted permittivity and permeability are smooth functions of τ , describing a homogenized behavior of the inhomogeneous material. Interestingly, ϵ_r peaks at a value greater than 10 when $\tau \approx 0.8$, while μ_r is slightly less than unity throughout the range of τ , reaching a minimum of 0.71 at $\tau \approx 0.65$. Note that the value of s_1 was chosen to make $|\Gamma| \leq 1$, and was found to

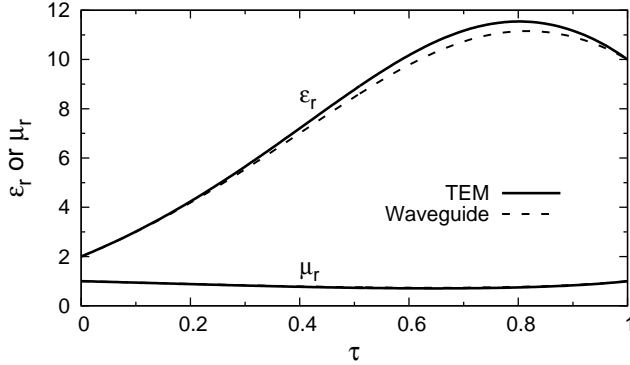


Figure 4. Permittivity and permeability for a layered dielectric sample. $f = 2$ GHz, $n = 0$.

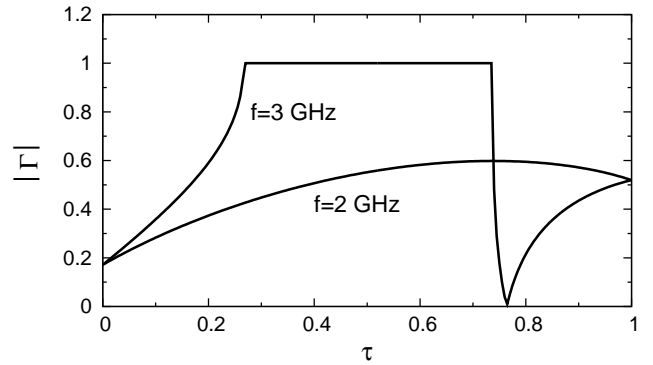


Figure 5. Reflection coefficient magnitude for a layered dielectric material in a TEM system.

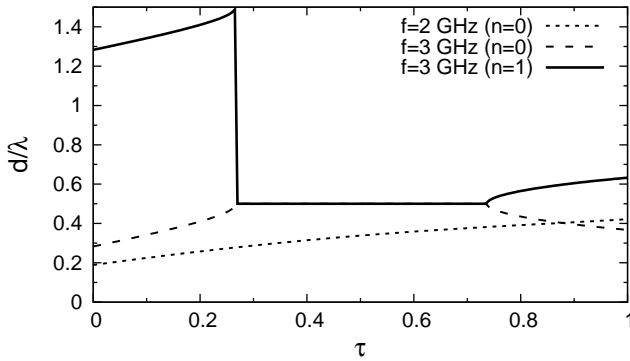


Figure 6. Sample thickness in wavelengths for a layered dielectric material in a TEM system.

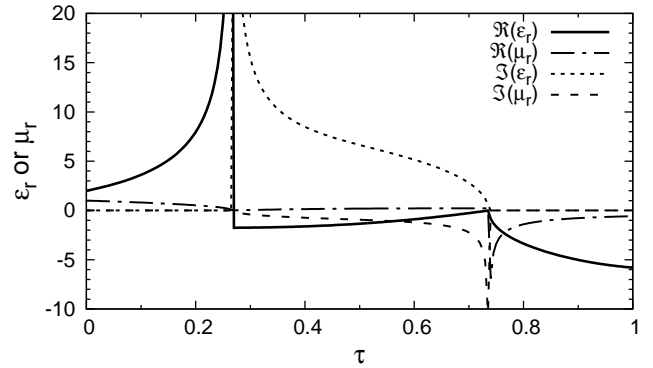


Figure 7. Permittivity and permeability for a layered dielectric material in a TEM system. $f = 3$ GHz, $n = 0$.

be $s_1 = 1$ for all values of τ . The resulting $|\Gamma|$ is shown in Figure 5. Using the extracted values of μ and ϵ it is possible to compute the homogenized wavelength as $\lambda = \lambda_0 / \sqrt{\mu_r \epsilon_r}$, where $\lambda_0 = c/f$. Figure 6 shows the thickness of the sample compared to this wavelength. Clearly, the sample is less than a half wavelength in thickness for all values of τ .

At $f = 3$ GHz, the plot of S_{11} is significantly more complicated. For $0 \leq \tau < 0.266$, S_{11} lies in the region where $X < -1$, and thus the extracted values of ϵ and μ must be real. For $0.267 \leq \tau \leq 0.736$, X lies in the range $-1 < X < 1$, and here μ and ϵ are complex. For $0.737 \leq \tau \leq 0.763$, $X > 1$ and for $0.764 \leq \tau \leq 1$, $X < -1$. Thus, ϵ and μ will again be real for $\tau \geq 0.737$. The values of s_1 and s_2 were chosen to keep $|\Gamma| \leq 1$. It was found that $s_1 = 1$ for $0 \leq \tau < 0.266$, $s_2 = 1$ for $0.267 \leq \tau \leq 0.736$, $s_1 = -1$ for $0.737 \leq \tau \leq 0.763$, and $s_1 = 1$ for $0.764 \leq \tau \leq 1$. Figure 5 shows a plot of $|\Gamma|$. As expected, $|\Gamma| = 1$ in the range $0.267 \leq \tau \leq 0.736$ where the extracted material parameters are complex, indicating a regime of total interfacial reflection.

The extracted values of μ and ϵ depend on the value of n chosen. Figure 7 shows μ and ϵ for $n = 0$. As predicted, for $0 \leq \tau < 0.266$ and for $0.737 \leq \tau \leq 1$ both ϵ and μ are real. In the range $0 \leq \tau < 0.266$ the homogenized values may be interpreted as those of an ordinary dielectric. The extracted value of ϵ_r is 2 at $\tau = 0$, as expected, but diverges as τ approaches 0.266. The extracted μ_r is unity at $\tau = 0$, again as expected, but μ_r becomes zero as τ approaches 0.266. In contrast, when $0.737 \leq \tau \leq 1$, both ϵ_r and μ_r are negative. Since $s_0 = -1$ and $s_1 = -1$ in this range, this is Case D of Table 3, indicating $0 < \phi < \pi$. Thus, the material may be interpreted as a lossless, double negative metamaterial if the thickness is less than half a wavelength. Computing $\lambda = \lambda_0 / \Re\{\sqrt{\mu_r \epsilon_r}\}$ from the extracted values of μ_r and ϵ_r produces the normalized thickness shown in Figure 6. Clearly, $d/\lambda < 0.5$ for the range $0.737 \leq \tau \leq 1$.

Setting $n = 1$ produces Figure 9. In this case the material has the expected homogenized behavior as an ordinary dielectric in the range $0.737 \leq \tau \leq 1$. The extracted ϵ_r varies from zero at $\tau = 0.737$ to the expected value of 10 at $\tau = 1$. Meanwhile μ_r diverges at $\tau = 0.737$ and achieves the expected value of unity at $\tau = 1$. Figure 6 shows that in this range (unlike for $n = 0$) the thickness is greater than a half wavelength. In the range $0 \leq \tau < 0.266$ the homogenized values may be interpreted as those of an ordinary dielectric with positive values of both ϵ_r and μ_r , but now the behavior of these parameters is not as expected as τ approaches zero. In the range $0.267 \leq \tau \leq 0.736$, both ϵ_r and μ_r are complex, regardless of n , and achieve opposite signs. Thus, values of ϵ and μ with expected behavior can only be extracted in the range $0 \leq \tau < 0.266$ using $n = 0$ and in the range $0.737 \leq \tau \leq 1$ using $n = 1$. Since $\Im\{\epsilon_r\} > 0$ for $n = 0$ and $\Im\{\mu_r\} > 0$ for $n = 1$ in the range $0.267 \leq \tau \leq 0.736$, no meaningful values of ϵ_r and μ_r may be extracted in this range.

An important conclusion may be drawn when the NRW method is used to characterize this lossless engineered material as a metamaterial. At $f = 3$ GHz, when $0.737 \leq \tau \leq 1$ exactly the same values of S_{11} and S_{21} are produced by an ordinary material with real positive values of ϵ_r and μ_r , and by a double negative material with real negative values of ϵ_r and μ_r . Which of these should be used to interpret the homogenized behavior of the layered material? This is a question that cannot be answered if only the S -parameters of the materials are of interest. Additional tests other than using NRW for the sample placed into a TEM system are required to address the ambiguous behavior of the material.

The question arises as to whether the extracted material parameters depend on the method of measurement. For a homogeneous sample, results are theoretically independent of whether the sample is measured in a free-space system, a TEM guided wave system, or a rectangular waveguide (except for some issues near half-wavelength frequency boundaries). To see the effect of the measurement system

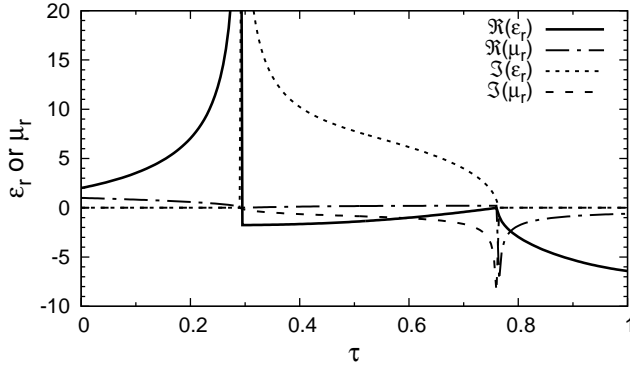


Figure 8. Permittivity and permeability for a layered dielectric material in a WR340 waveguide. $f = 3$ GHz, $n = 0$.

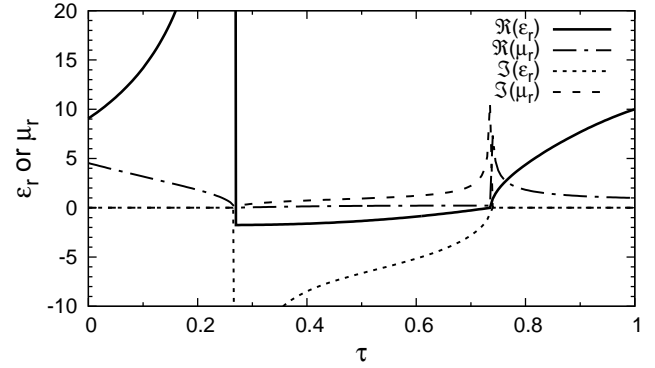


Figure 9. Permittivity and permeability for a layered dielectric material in a TEM system. $f = 3$ GHz, $n = 1$.

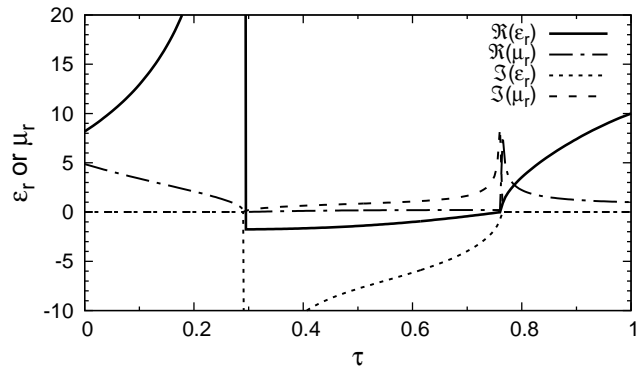


Figure 10. Permittivity and permeability for a layered dielectric material in a WR340 waveguide. $f = 3$ GHz, $n = 1$.

on the properties of an engineered material, the same layered sample considered above is placed into a WR-340 rectangular waveguide with $a = 3.4$ inches (86.36 mm). The S -parameters, computed using a cascaded layer approach, are shown in Figure 3 for $f = 2$ GHz and $f = 3$ GHz. Values of S_{11} are quite similar to those for the TEM system shown in Figure 2. The curve is somewhat displaced for $f = 2$ GHz, but remains entirely within the circle defined by $X^2 > 1$. Thus, the permittivity and permeability are purely real at this frequency, as seen in Figure 4. In fact, the values differ only slightly from those found using a TEM system. The S_{11} curve is also somewhat shifted for $f = 3$ GHz, but the extracted permittivity and permeability for both $n = 0$ and $n = 1$ are very similar to those for a TEM system, as seen in Figures 8 and 10. Note that the transitions from $X^2 > 1$ to $X^2 < 1$ occur at slightly different values of τ compared to the TEM case.

5. EXAMPLE 2: WAVEGUIDE IRIS

As a second example, consider the experimental S -parameters of a rectangular iris placed in an X-band rectangular waveguide. The waveguide is WR-90 with dimensions $a = 0.9$ inch by $b = 0.4$ inch (22.86 by 10.16 mm). The iris consists of a 0.125 inch (3.175 mm) thick metallic section with an opening 0.125 inches (3.175 mm) tall located at the top of the section. The iris was constructed by creating a flange on a 3-D printer using “Vero White” polymer, largely a mixture of poly(isobornyl acrylate) and poly(methyl methacrylate). The printer is a Stratasys Objet Connex350 with a repeatable print resolution of approximately 16 μm . The printed plastic has approximately 10 μm of surface roughness. The printed part was sputter coated with 100 nm of titanium followed by 2 μm of copper (about three skin depths at 10 GHz). The flange includes both bolt holes and holes for precision alignment pins, as shown in Figure 11. The flange was bolted between two WR90 waveguide sections of length 6 inches (152.4 mm) and the S -parameters were measured using an Agilent E5071C ENA vector network analyzer with a 3-short calibration. The S -parameters measured at the ends of the waveguide sections were phase-shifted to the plane of the iris to determine the S -parameters of the iris. Thus, the transformed S -parameters only involve the dominant mode amplitude, even though higher-order mode fields are present near the iris. See Figure 12 for a diagram of the experimental setup.

Whether the measured S -parameters satisfy the conditions for a lossless network can be tested by using Eq. (20). If the system is lossless, the quantity $1 - |S_{11}|^2 - |S_{21}|^2$ will be zero. This quantity is plotted in Figure 15, and found to vary from around 0.03 at the low end of the band, to near zero at the high end. Thus, the S -parameters describe a slightly lossy network. This is probably due to losses in the copper, possibly exacerbated by the roughness of the surface and uneven sputtering of copper.

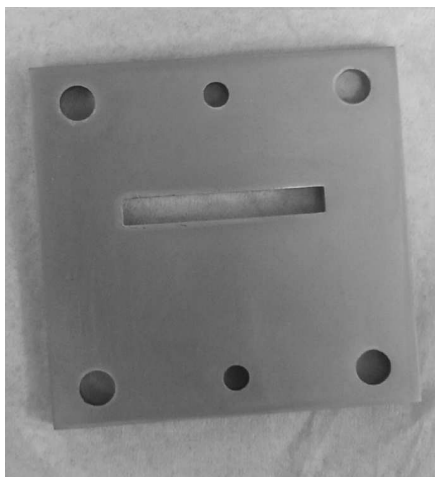


Figure 11. Waveguide iris created using 3-D printed plastic flange sputtered with copper.

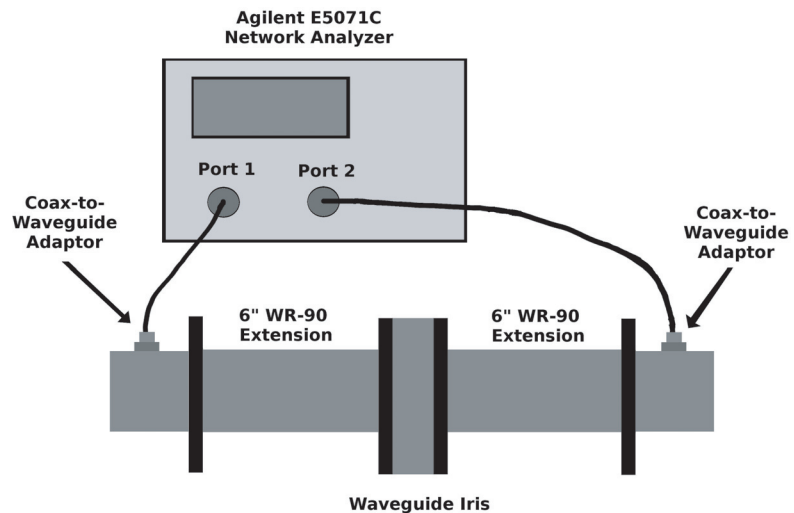


Figure 12. Experimental setup used to measure the S -parameters of the waveguide iris.

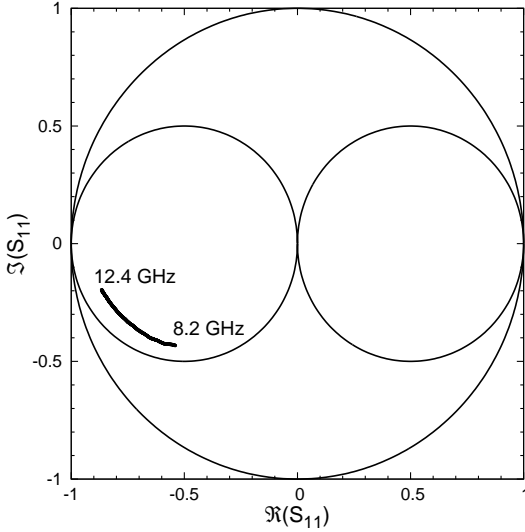


Figure 13. Measured values of S_{11} for an iris in X-band waveguide.

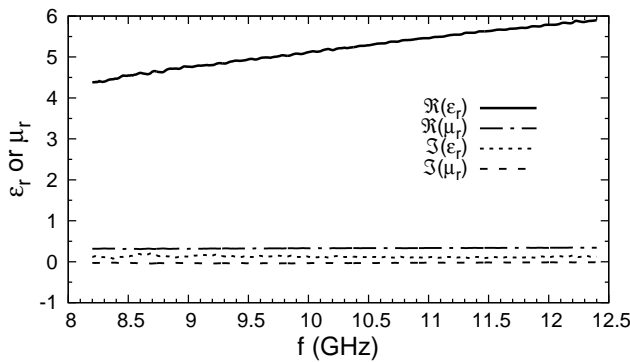


Figure 14. Permittivity and permeability extracted from measurements of an iris in X-band waveguide. $n = 0$.

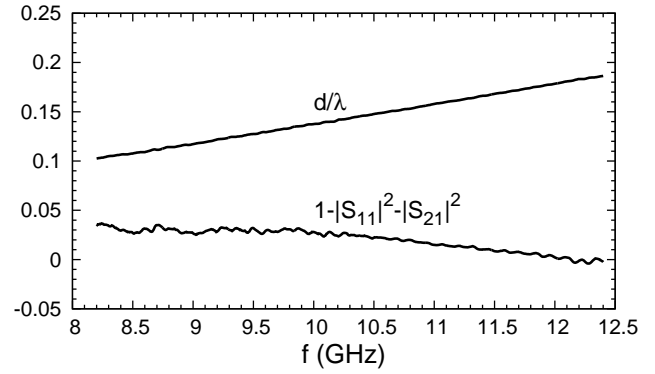


Figure 15. Electrical thickness and power balance for a waveguide iris in X-band waveguide. $n = 0$.

The measured values of S_{11} are shown in Figure 13. It is seen that these measurements fall into the region where $X^2 > 1$, and thus the extracted imaginary values of μ and ϵ would be zero if the network were truly lossless. Figure 14 shows the actual values extracted using the NRW method assuming the iris is a homogeneous material. The real part of the extracted value of μ is fairly constant across the band with real $\mu_r \approx 0.3$, while real ϵ varies smoothly from about $\Re\{\epsilon_r\} = 4.5$ to $\Re\{\epsilon_r\} = 6$. The extracted imaginary parts of the permittivity and permeability are small but nonzero, with $\Im\{\epsilon_r\}$ varying from a low of about 0.07 to a high of 0.2 and $\Im\{\mu_r\}$ varying from a low of about -0.04 to a high of -0.01. Note that the positive value for the imaginary part of ϵ does not violate energy conservation, since the NRW method assumes the sample to be homogeneous, which it is not. All parameters were extracted using $n = 0$. This choice is justified by computing the electrical thickness of the iris using $\lambda = \lambda_0 / \Re\{\sqrt{\mu_r \epsilon_r}\}$ from the extracted values of μ_r and ϵ_r , producing the result shown in Figure 15. Clearly $d/\lambda < 0.5$ over the measurement band.

6. EXAMPLE 3: METAMATERIAL WAVEGUIDE INSERT

As an example of a structure that has appreciable loss, consider a waveguide insert designed to have a negative permeability over a portion of F-band. The insert consists of a 16×16 array of square copper

pixels, each of size 0.5×0.5 mm, etched onto 0.78 mm thick Rogers 5879 RT/duroid with dielectric constant $\epsilon_r = 2.33$ and loss tangent $\delta = 0.0012$. A genetic algorithm was used to turn on the presence of various pixels such that permeability near 5.5 GHz, when extracted using the NRW method, has a negative real part [24]. Pixels were placed both on the front and back surfaces of the insert, so that the back surface is a reverse mirror image of the front, and the structure is symmetric when placed into a waveguide (i.e., $S_{11} = S_{22}$). The front surface of the resulting pixelated structure is shown in Figure 16.

The S -parameters of the waveguide insert were simulated using HFSS across the band 5–6 GHz with the insert placed along the centerline of WR159 rectangular waveguide (40.386 by 20.193 mm), with S_{11} plotted in Figure 17. The insert is not lossless, and both copper and substrate loss are included in the simulation. However, the loss is small enough that the analysis developed earlier is very useful in predicting the behavior of the extracted material parameters. From Figure 17 it is seen that $X^2 > 1$ in the frequency ranges $5 < f < 5.61$ GHz and $5.77 < f < 6$ GHz. Thus, if the insert were lossless, both ϵ and μ would be purely real in these frequency ranges. For $5.61 < f < 5.77$ GHz, $X^2 < 1$, and thus in this frequency range a lossless insert would produce complex values of ϵ and μ , with the imaginary parts having opposite signs. Instead of these expected abrupt transitions (as were seen in the case of the layered dielectric example), the presence of loss produces a smoother transition across the frequency boundaries, but the behavior is still much as is predicted.

Figure 18 shows the values of ϵ and μ extracted from the simulated S -parameters using the NRW method with $n = 0$, and assuming the insert is homogeneous. It is seen for $5 < f < 5.5$ GHz and for $5.8 < f < 6$ GHz the imaginary parts of μ and ϵ are very small, but non-zero, with a smooth transition into a region where the structure undergoes a strong resonance. In this region, between approximately 5.6 and 5.75 MHz, $\Re\{\mu\}$ passes through zero and becomes negative, while $\Im\{\mu\}$ becomes highly negative. Both $\Re\{\epsilon\}$ and $\Im\{\epsilon\}$ remain positive throughout the resonance region, except for a very small range around 5.75 GHz where $\Re\{\epsilon\}$ is slightly less than zero. Thus, as predicted by the analysis presented earlier, the imaginary parts of μ and ϵ have opposite signs within the resonance band.

The effect of negative μ is to produce a frequency range where the propagation constant of the dominant waveguide mode is real and negative, the wave is evanescent, and there is no power transmission. This is clearly observed in Figure 19, which shows the magnitudes of the simulated S -parameters. The value of $|S_{21}|$ is significantly reduced in the resonance region $5.6 < f < 5.75$ GHz,

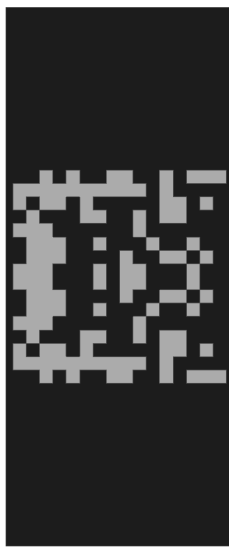


Figure 16. Metamaterial waveguide insert.

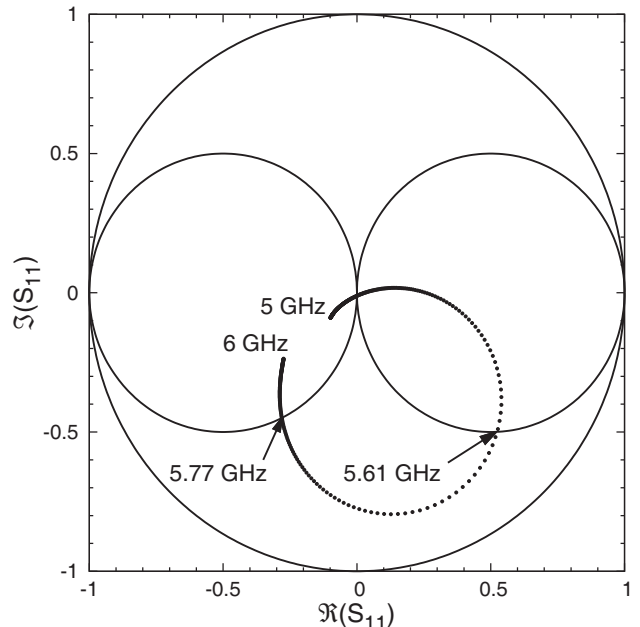


Figure 17. Simulated values of S_{11} for a metamaterial insert in F-band waveguide.

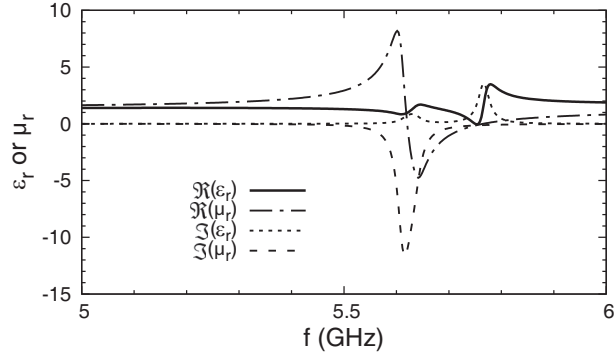


Figure 18. Permittivity and permeability extracted from the simulated S -parameters of a metamaterial insert in F-band waveguide. $n = 0$.

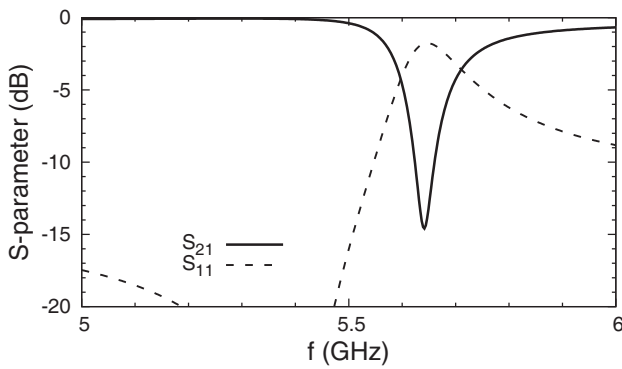


Figure 19. Magnitude of measured S -parameters for a metamaterial waveguide insert.

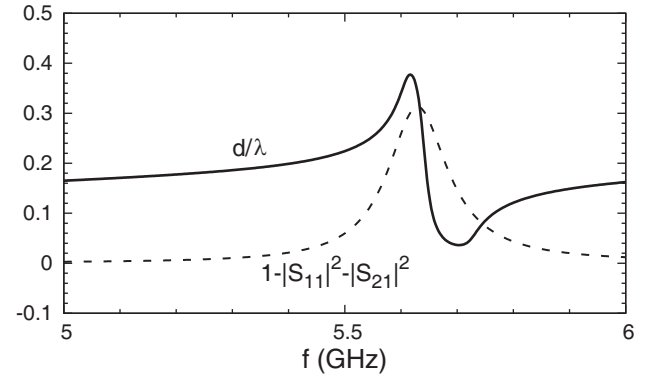


Figure 20. Electrical thickness and power balance for a metamaterial waveguide insert. $n = 0$.

where $\Re\{\mu\} < 0$. This is also the region where structure loss is most significant as revealed by the power balance curve plotted in Figure 20. Figure 20 also shows the electrical thickness of the insert found using $\lambda = \lambda_0 / \Re\{\sqrt{\mu_r \epsilon_r}\}$ from the extracted values of μ_r and ϵ_r . Note that with $n = 0$ the electrical length is never greater than 0.4λ . Interestingly, at the upper end of the resonance region the electrical length becomes very small, since λ increases dramatically at the point where $\epsilon_r \approx 0$.

The bandstop behavior of the insert can be used to produce a waveguide filter with desirable properties. By using several carefully designed pixelated structures, the stop band can be increased, and the skirts made quite sharp [25].

7. CONCLUSION

Relationships between the measured S -parameters of an engineered material and the permittivity and permeability of the material are derived by examining the closed-form expressions of the Nicolson-Ross-Weir method. The conditions under which the extracted material properties may be associated with a lossless material are deduced. Also identified are the relationship between the signs of the real and imaginary parts of the permittivity and permeability, when the extracted material parameters are either real or complex. Although the expressions are only truly valid when the material is lossless, it is possible to use the expressions to understand and predict the behavior of engineered materials with low to moderate loss, as demonstrated by considering the example of a metamaterial waveguide insert. The derived relationships between the material characteristics and the S -parameters should prove useful when synthesizing materials to have certain desired properties.

REFERENCES

1. Nicolson, A. M. and G. F. Ross, "Measurement of the intrinsic properties of materials by time-domain techniques," *IEEE Trans. Instrum. Meas.*, Vol. 19, No. 4, 377–382, 1970.
2. Weir, W. B., "Automatic measurement of complex dielectric constant and permeability at microwave frequencies," *Proc. IEEE*, Vol. 62, No. 1, 33–36, 1974.
3. Baker-Jarvis, J., M. D. Janezic, J. H. Grosvenor, and R. G. Geyer, "Transmission/reflection and short-circuit line methods for measuring permittivity and permeability," Tech. Note 1355, National Institute of Standards and Technology, Dec. 1993.
4. Chen, L. F., C. K. Ong, C. P. Neo, V. V. Varadan, and V. K. Varadan, *Microwave Electronics: Measurement and Materials Characterization*, John Wiley & Sons Ltd., West Sussex, England, 2004.
5. Morales, C., J. Dewdney, S. Pal, S. Skidmore, K. Stojak, H. Srikanth, T. Weller, and J. Wang, "Tunable magneto-dielectric polymer nanocomposites for microwave applications," *IEEE Trans. Microw. Theory Tech.*, Vol. 59, No. 2, 302–310, 2011.
6. Balaabed, B., J. L. Wojkiewicz, S. Lamoun, N. El Kamchi, and T. Lasri, "Synthesis and characterization of hybrid conducting composites based on polyaniline/magnetite fillers with improved microwave absorption properties," *J. Alloys and Compounds*, Vol. 527, 137–144, Jun. 25, 2012.
7. Soleimani, H., Z. Abbas, N. Yahya, H. Soleimani, and M. Y. Ghotbi, "Determination of complex permittivity and permeability of lanthanum iron garnet filled PVDF-polymer composite using rectangular waveguide and Nicholson-Ross-Weir (NRW) method at X-band frequencies," *Measurement*, Vol. 45, 1621–1625, 2012.
8. Wang, L., R. Zhou, and H. Xin, "Microwave (8–50 GHz) characterization of multiwalled carbon nanotube papers using rectangular waveguides," *IEEE Trans. Microw. Theory Tech.*, Vol. 56, No. 2, 499–506, 2008.
9. Katsounaros, A., K. Z. Rajab, Y. Hao, M. Mann, and W. I. Milne, "Microwave characterization of vertically aligned multiwalled carbon nanotube arrays," *Applied Phys. Lett.*, Vol. 98, 203105/1–203105/3, 2011.
10. Havrilla, M. J. and D. P. Nyquist, "Electromagnetic characterization of layered materials via direct and de-embed methods," *IEEE Trans. Inst. Meas.*, Vol. 55, No. 1, 158–163, 2006.
11. Ziolkowski, R. W., "Design, fabrication, and testing of double negative metamaterials," *IEEE Trans. Ant. Propag.*, Vol. 51, No. 7, 1516–1529, 2003.
12. Alu, A., "First-principles homogenization theory for periodic metamaterials," *Phys. Rev. B*, Vol. 84, 075153/1–075153/18, 2010.
13. Hasar, U. C., J. J. Barroso, C. Sabah, I. Y. Ozbek, Y. Kaya, D. Dal, and T. Aydin, "Retrieval of effective electromagnetic parameters of isotropic metamaterials using reference-plane invariant expressions," *Progress In Electromagnetics Research*, Vol. 132, 425–441, 2012.
14. Karamanos, T. D., A. I. Dimitriadi, and N. V. Kantartzis, "Compact double-negative metamaterials based on electric and magnetic resonators," *IEEE Ant. Wireless Propag. Lett.*, Vol. 11, 480–483, 2012.
15. Majid, H. A., M. K. A. Rahim, and T. Masri, "Microstrip antenna's gain enhancement using left-handed metamaterial structure," *Progress In Electromagnetics Research M*, Vol. 8, 235–247, 2009.
16. Singhal, P. K. and B. Garg, "Design and characterization of compact microstrip patch antenna using 'split ring' shaped metamaterial structure," *International Journal of Electrical and Computer Engineering*, Vol. 2, No. 5, 655–662, 2012.
17. Zani, M. Z. M., M. H. Jusoh, A. A. Sulaiman, N. H. Baba, R. A. Awang, and M. F. Ain, "Circular patch antenna on metamaterial," *Intl. Conf. on Electronic Devices, Systems and Applications (ICEDSA)*, 313–316, Kuala Lumpur, Malaysia, April 11–14, 2010.
18. Crowgey, B. R., J. Tang, E. J. Rothwell, B. Shanker, and L. C. Kempel, "A waveguide verification standard design procedure for the microwave characterization of magnetic materials," *Progress In*

Electromagnetics Research, Vol. 150, 29–40, 2015.

- 19. Wang, Y., Z. Duan, X. Tang, Z. Wang, Y. Zhang, J. Feng, and Y. Gong, “All-metal metamaterial slow-wave structure for high-power sources with high efficiency,” *Applied Physics Letters*, Vol. 107, No. 15, 1, Oct. 2015.
- 20. Faraji, H. S., G. Atmatzakis, M. F. Su, and C. G. Christodoulou, “Creating double negative index metallic materials for HPM applications,” *Proc. AMEREM 2014*, ID 124, Albuquerque, NM, Jul. 27–31, 2014.
- 21. Arslanagic, S., T. V. Hansen, N. A. Mortensen, A. H. Gregersen, O. Sigmund, R. W. Ziolkowski, and O. Breinbjerg, “A review of the scattering-parameter extraction method with clarification of ambiguity issues in relation to metamaterial homogenization,” *IEEE Antennas and Propagation Magazine*, Vol. 55, No. 2, 91–106, 2013.
- 22. Sihvola, A., “Metamaterials in electromagnetics,” *Metamaterials*, Vol. 1, No. 1, 2–11, 2007.
- 23. Helszajin, J., *The stripline Circulator: Theory and Practice*, John Wiley & Sons, New York, 2008.
- 24. Ouedraogo, R. O., “Topology optimization of metamaterials and their applications to RF component design,” Ph.D. Dissertation, Michigan State University, East Lansing, MI, May 2011.
- 25. Ouedraogo, R. O., E. J. Rothwell, A. R. Diaz, K. Fuchi, and J. Tang, “Waveguide band-stop filter design using optimized pixelated inserts,” *Microwave and Optical Technology Letters*, Vol. 55, No. 1, 141–143, 2013.